

Effect of Blend Composition and Additives on the Morphology of PCPDTBT:PC₇₁BM Thin Films for Organic Photovoltaics

Christoph J. Schaffer, Johannes Schlipf, Efi Dwi Indari, Bo Su, Sigrid Bernstorff,[†] and Peter Müller-Buschbaum*

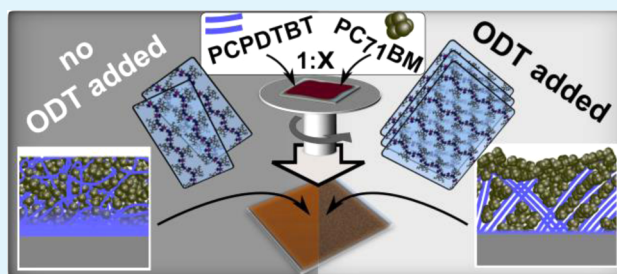
Lehrstuhl für Funktionelle Materialien, Physik-Department, Technische Universität München, James-Frank-Strasse 1, 85748 Garching, Germany

[†]Elettra–Sincrotrone Trieste S.C.p.A., Strada Statale 14 - km 163.5 in AREA Science Park, Basovizza, 34149 Trieste, Italy

S Supporting Information

ABSTRACT: The use of solvent additives in the fabrication of bulk heterojunction polymer:fullerene solar cells allows to boost efficiencies in several low bandgap polymeric systems. It is known that solvent additives tune the nanometer scale morphology of the bulk heterojunction. The full mechanism of efficiency improvement is, however, not completely understood. In this work, we investigate the influences of blend composition and the addition of 3 vol % 1,8-octanedithiol (ODT) as solvent additive on polymer crystallization and both, vertical and lateral morphologies of poly[2,6-(4,4-bis(2-ethylhexyl)-4H-cyclopenta [2,1-b;3,4-b']dithiophene)-*alt*-4,7(2,1,3-benzothiadiazole)] and [6,6]-phenyl C₇₁-butyric acid methyl ester (PCPDTBT:PC₇₁BM) blend thin films processed from chlorobenzene-based solutions. The nanoscale morphology is probed with grazing incidence small- and wide-angle X-ray scattering as well as X-ray reflectivity and complemented with UV/vis spectroscopy. In PCPDTBT:PC₇₁BM films the use of ODT is found to lower the solubility of fullerene in the polymer matrix and to promote polymer crystallization, both vertical and lateral microphase separation with morphological coarsening, and formation of a fullerene-rich topping layer. The enhanced photovoltaic performance is explained by these findings.

KEYWORDS: GISAXS, GIWAXS, organic photovoltaics, morphology, solvent additive, bulk-heterojunction, ODT, PCPDTBT



1. INTRODUCTION

For approaching the launch of polymer-based organic photovoltaics (OPV) into the renewable energy sector, improving device efficiency and stability has turned out to be the most important challenges in the last years. In this context, the concept of bulk heterojunction (BHJ) architecture has shown a highly promising framework providing several advantages.¹ Among them, mechanical flexibility and low weight,² potential optical transparency,^{3,4} and the capability of production on a large scale by roll-to-roll printing,⁵ as well as by spin coating on a laboratory scale,⁶ particularly render OPV devices a highly versatile source of electricity. As a more recent method, spray deposition has been implemented for OPV fabrication.⁷ In polymer-based bulk heterojunction solar cells, an active blend layer, which typically consists of a suitable polymer and a solvable fullerene derivative, is applied from a mutual solution via one of these deposition techniques. As its components demix during film solidification, pure polymer and pure fullerene domains on a nanometer length scale form within a partially mixed amorphous phase of polymer and fullerene.⁸ In a working solar cell, pure domains shape an interpenetrating network. The morphology of the forming bulk heterojunction layer is hereby crucial for the functioning of the solar device, as only excitons that are closer to an inter domain interface of the

interpenetrating BHJ network than the exciton diffusion length in the polymer (~10 nm) can contribute to current generation.^{9,10} A more complete discussion of OPV device physics can be found in literature.^{11–14} As the exact morphology found in the active layer matters strongly, tuning it has shown to allow for a significant increase of solar cell performance. To optimize the nanoscale morphology, several strategies have been reported. Among them are thermal annealing,^{15–18} solvent annealing,¹⁹ a careful choice of solvents,²⁰ and the use of solvent additives.^{21,22} Solar cells can further be improved by combining such techniques with the use of so-called low-bandgap polymers which possess absorption spectra that match with the solar spectrum. For the specific system of poly[2,6-(4,4-bis(2-ethylhexyl)-4H-cyclopenta [2,1-b;3,4-b']dithiophene)-*alt*-4,7(2,1,3-benzothiadiazole)] and [6,6]-phenyl C₇₁-butyric acid methyl ester (PCPDTBT:PC₇₁BM), solvent additives lead to a strong improvement. Peet et al. have shown that the overall power conversion efficiency was enhanced from 2.5 to 5.8% by use of a few volume percent of 1,8-octanedithiol (ODT) as solvent

Received: July 2, 2015

Accepted: September 10, 2015

Published: September 10, 2015

additive in chlorobenzene (CB).²² Moreover, a former investigation on poly(3-hexylthiophene) (P3HT):PC₆₁BM revealed that the addition of small amounts of alkanethiols affected phase segregation and lead to enhanced polymer aggregation, and hence to an improved charge carrier mobility in the polymer.²³ In this context, it has been shown by Gu et al. that the use of ODT as solvent additive for a C₆₀-based PCPDTBT:PC₆₁BM blend resulted in an enhanced polymer crystallinity as well as in an enhanced phase segregation.²⁴ It is commonly expected that such a mechanism, if applicable to the blend system based on C₇₀ fullerene, i.e., PCPDTBT:PC₇₁BM, could also explain the enhanced OPV efficiency reported by Peet et al.²² However, a comprehensive structural investigation on the influence of ODT on the inner morphology of the blend system of PCPDTBT and PC₇₁BM thin films is yet due and of particularly high interest, as most reported BHJ solar cells with highly efficient low-bandgap polymers, such as PCDTBT, PCPDTBT, Si-PCPDTBT, or PTB7, rely on PC₇₁BM instead of PC₆₁BM as electron acceptor.^{21,22,25–27}

Thus, in this work, we provide a systematic investigation on the inner morphology of thin films from PCPDTBT:PC₇₁BM with different blend ratios (1:1.5, 1:2.0, and 1:2.7), cast from CB with and without adding 3 vol % (2.9 wt %) ODT. We investigate the crystalline order in the different films by means of grazing incidence wide-angle X-ray scattering (GIWAXS) and UV/vis spectroscopy.^{28–32} X-ray reflectometry (XRR) gives insight into the actual composition and the vertical structure of the thin films. Finally, the enhancement of microphase separation by ODT is evidenced by grazing incidence small-angle X-ray scattering (GISAXS).²⁸ The results are discussed in the context of their impact on the photo conversion properties of PCPDTBT:PC₇₁BM-based solar cells.

2. EXPERIMENTAL SECTION

Sample Preparation. Thin films have been prepared by spin coating on silicon (X-ray analysis) and glass (UV/vis) substrates, which have been cleaned with an acid treatment and carefully rinsed just before film application.³³ Solutions were prepared from chlorobenzene (chlorobenzene:ODT, 3% vol.) at a fixed total concentration of 25 mg/mL with different weight fractions (1:1.5, 1:2.0, and 1:2.7) of poly[2,6-(4,4-bis(2-ethylhexyl)-4H-cyclopenta[2,1-b;3,4-b']dithiophene)-alt-4,7(2,1,3-benzothiadiazole)] and [6,6]-phenyl C₇₁-butyric acid methyl ester (PCPDTBT:PC₇₁BM). PCPDTBT ($M_w = 31$ kDa, PDI = 1.9) and PC₇₁BM were purchased from ONE Material and used as received. The samples were measured after spin-casting without any additional annealing or drying step.

UV/vis Spectroscopy. The absorbance for all films was measured with an UV–vis spectrometer Lambda35 (PerkinElmer) using a scanning speed of 120 nm/min and a slit width of 2 nm, in transmission mode using a sampling resolution of 1 nm. All measurements were corrected for the cleaned glass substrate.

GISAXS/GIWAXS. Grazing incidence small-angle X-ray scattering (GISAXS) and grazing incidence wide-angle X-ray scattering (GIWAXS) measurements were performed at the Austrian SAXS beamline of the Elettra Sincrotrone in Trieste, Italy, at a photon energy of 8 keV (0.154 nm). For GISAXS a sample–detector distance of 2.05 m (104 mm for GIWAXS) and an incident angle of $\alpha_i = 0.4^\circ$ (0.25° for GIWAXS) were chosen. Data were measured with a DECTRIS PILATUS3 1M (GISAXS) and 100k detector (GIWAXS). GISAXS data were recorded for 10×20 s and summed for a total acquisition time of 200 s. Beam damage was ruled out by sequentially comparing the single GISAXS measurements, because no changes within the different single measurements was found. GIWAXS exposure time was 100 s.

XRR. X-ray reflectivity (XRR) measurements were performed on a single batch of samples in house with a Bruker Advance D8

reflectometer, using the K α line at 8048 eV and slit widths of (0.2/0.2/0.05) mm, yielding a resolution of about $\Delta q/q = 1.5\%$. Fitting of the XRR data was performed with the Motofit package by Nelson et al.⁴¹

3. RESULTS AND DISCUSSION

3.1. Polymer Crystallites. Crystallite Structure. Detailed information on crystallites in PCPDTBT:PC₇₁BM thin films with different blend ratios (1:1.5, 1:2.0, and 1:2.7 PCPDTBT:PC₇₁BM) processed from CB and CB with 3 vol % ODT is extracted from GIWAXS measurements. Figure 1 shows 2D GIWAXS data of the films without (upper row) and with (lower row) use of ODT.

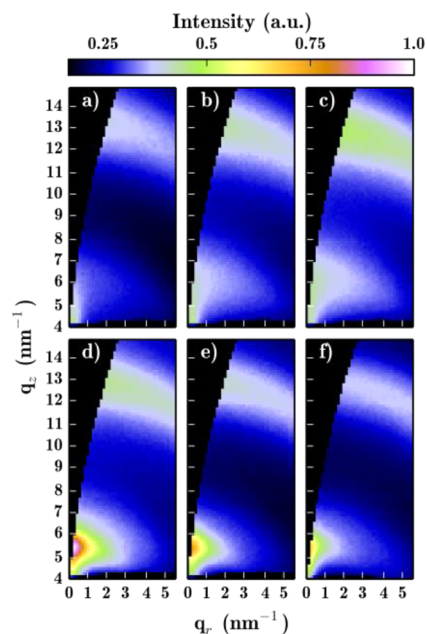


Figure 1. 2D GIWAXS data of PCPDTBT:PC₇₁BM thin films without ODT ((a) 1:1.5, (b) 1:2.0, (c) 1:2.7) and of films with ODT ((d) 1:1.5, (e) 1:2.0, (f) 1:2.7). The Bragg peak at $q_z \approx 5.5$ nm⁻¹ corresponds to the 100 lamellar stacking of PCPDTBT. The ring-like pattern around $q_z \approx 13$ nm⁻¹ arises from PC₇₁BM aggregates.

All GIWAXS data have been corrected for the setup geometry and remapped on a q_r – q_z representation which accounts for the lacking sensitivity for q_z at $q_r = 0$ using GIXSGUI.^{30,34} The Bragg peak located around 5.5 nm⁻¹ is strongly enhanced by the use of ODT. It corresponds to the (100) reflection of the lamellar PCPDTBT stacking along the alkyl chains which was reported to display around 1.2 nm stacking distance.³² For a more detailed analysis, cake cuts are integrated over an angular range of 5–15° with respect to the specular plane. The resulting integrated intensities versus the scattering vector q are shown in Figure 2.

The most prominent reflex (left arrow in Figure 2a) at 5.5 nm⁻¹ appears only when ODT is used. The second prominent peak is located at 13 nm⁻¹ (middle arrow in Figure 2a) and we identify a third, weak intensity feature around 18.5 nm⁻¹ (right arrow in Figure 2a). For further analysis the curves are fitted (red lines in Figure 2a) by a superposition of three Lorentzian-shaped peaks, representing the three observed features in the data. The background is hereby handled by an exponential decay contribution for elimination of the SAXS tail.³⁵ Using such a model function, we extract the peak center positions and

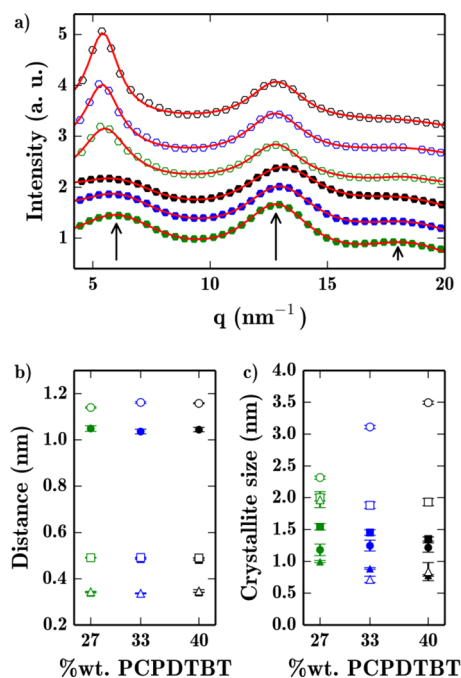


Figure 2. GIWAXS analysis: Open symbols correspond to the films with ODT and filled symbols to those without ODT addition. Different colors denote the different PCPD/TBT:PC₇₁BM blend ratios (black, 1:1.5 (40 wt % PCPD/TBT); blue, 1:2.0 (33 wt % PCPD/TBT); green, 1:2.7 (27 wt % PCPD/TBT)). (a) Integrated GIWAXS data (5–15° cake cut around the sample surface normal). The data have been corrected for the detector setup geometry. Characteristic features are marked with arrows. PCPD/TBT contents from top to bottom: 40% w/ODT, 33% w/ODT, 27% w/ODT, 40% w/o ODT, 33% w/o ODT, 27% w/o ODT. (b) Stacking distances and (c) crystallite correlation lengths as obtained from the cake cut analysis. Dots denote lamellar crystallization of PCPD/TBT, squares refer to PC₇₁BM aggregation and triangles denote PCPD/TBT π - π stacking.

the full width half maxima of the Lorentzian-shaped peaks. These features allow for drawing conclusions on intermolecular distances and for a rough estimation of crystallite sizes. Intermolecular distances d are calculated from the peak center positions q_c via $d = 2\pi/q_c$ and the crystallite sizes L are estimated from the Scherrer equation, eq 1

$$L = \frac{0.9\lambda}{\Delta_{\text{FWHM}} \cos(\Theta)} \quad (1)$$

Hereby, λ denotes the X-ray wavelength, Θ the Bragg angle, and Δ_{fwhm} the reflex full width at half-maximum around the center of the scattering angle 2Θ . Within this model, fitting reveals the crystallite spacings and sizes given in Figure 2b, c (full set of parameters in Table S1). For the whole analysis of crystallite sizes, it must be noted that the validity of the

Scherrer formula for very small crystallites is still under discussion. Therefore, the absolute crystallite sizes might not be accurate. However, we believe that the deduced crystallite sizes allow for a relative comparison between the different samples investigated. All extracted parameters are shown in Table 1.

The full set of (stacking) distances d and correlation lengths L is given in Table 1. d_1/L_1 and d_3/L_3 correspond to distances/correlation lengths in lamellar and π - π stacks, respectively. d_2 and L_2 describe fullerene agglomerates. All lengths are given in Angstroms, errors are estimated from fitting tolerances.

The peak at 5.5 nm^{-1} originates from a crystal spacing of 11.5 \AA in case ODT is used (open circles in Figure 2b), which is in good agreement with literature.³² This distance is independent of the fullerene content. Crystallites are found to span over 2–3 lamella, whereas the size grows with an increasing polymer fraction in the blend (see open circles in Figure 2c). In case no ODT is used, we find a rather broad intensity halo and smaller lamellar stacking distance of 10.4 \AA . The crystallite sizes are hereby around one lamellar distance and therefore suggest that the polymer requires the solvent additive to crystallize at all. On the basis of the difference in stacking distances, we suggest that ODT leads to stretching of side chains, thus allowing for crystallization. In this case, fullerene molecules must be expelled from polymer domains.

This scenario is compatible with the information gained from the second peak in the GIWAXS data at around 13 nm^{-1} , which is found in the literature and regards the fullerene moiety of the film.³² A crystallite size or PC₇₁BM of 19.4 \AA is found for all blend ratios when ODT is used. Without ODT, this value is always smaller and shows a stronger dependence on the film composition. It increases from 13.5 to 15.4 \AA with increasing fullerene weight fraction, which supports the model where ODT pushes out fullerene molecules from polymer domains. The peak center position reveals a distance of around 4.9 \AA both without and with ODT. Because this length is smaller than the double C₇₀ fullerene radius, given by roughly $2 \times 4 \text{ \AA}$,³⁶ we attribute the peak to the distance of two opposite faces of neighboring fullerene molecules.

The third feature in the GIWAXS data around 18.5 nm^{-1} reveals a stacking distance of 3.4 \AA in both cases with and without ODT. This length scale is typical for π - π stacking in conducting polymers.^{37,38} The peak width reveals, that the crystallite extension in π - π direction reaches over roughly 2 (6 for the 1:2.7 ratio) polymer chains when ODT is used, and grows from 2 to 3 stacking distances with decreasing polymer fraction in the case where no ODT is used. This result might be counterintuitive because it suggests that films without ODT show a higher crystallite quality in π - π direction, which in turn would favor an efficient charge transport within the polymer moiety. Furthermore, it predicts an increasing polymer

Table 1. Full Set of Extracted Quantities from GIWAXS: d_1 , d_2 , d_3 Crystallite Spacings and L_1 , L_2 , L_3 Corresponding Crystallite Sizes

sample	d_1	d_2	d_3	L_1	L_2	L_3
1:1.5	10.4(1)	4.80(1)	3.41(1)	12.2(7)	13.5(4)	7.8(2)
1:2.0	10.4(1)	4.85(1)	3.38(1)	12.5(9)	14.5(4)	8.9(2)
1:2.7	10.5(2)	4.90(1)	3.39(1)	11.8(9)	15.4(5)	10.0(2)
1:1.5 ODT	11.6(1)	4.90(1)	3.47(6)	35.0(3)	19.3(6)	8.4(2)
1:2.0 ODT	11.6(1)	4.92(1)	3.37(2)	31.1(3)	18.8(5)	7.2(5)
1:2.7 ODT	11.4(1)	4.91(1)	3.44(3)	23.2(3)	20.0(5)	20(2)

crystallite quality for ODT-free blends with decreasing polymer content. To understand these findings, the crystallite quality is deduced from optical spectroscopy.

Crystallite Quality. To support the findings from GIWAXS, we investigate the crystallite quality within the different films by means of exciton bandwidths. Therefore, UV/vis experiments in transmission mode have been performed. Absorption data are shown in Figure 3a.

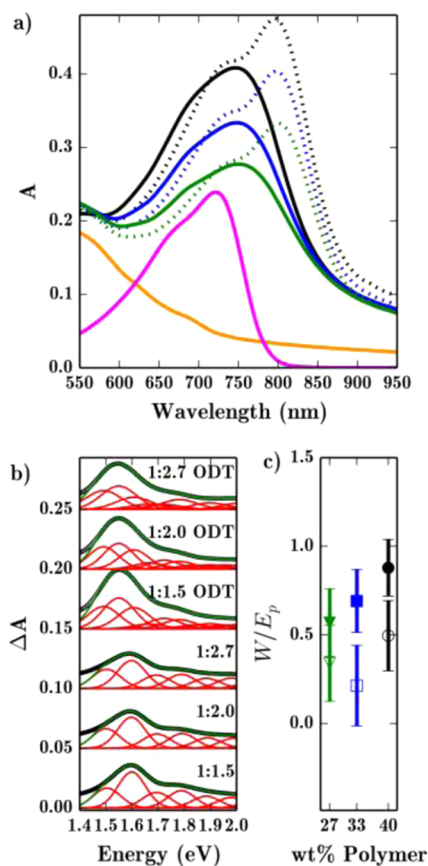


Figure 3. UV/vis absorption spectra. (a) Absorbance of PCPDTBT:PC₇₁BM thin films with polymer:fullerene ratios of 1:1.5 (black), 1:2.0 (blue), and 1:2.7 (green) without (solid lines) and with ODT (dotted lines). The orange and magenta lines show scaled absorbance spectra of PC₇₁BM (film) and PCPDTBT (solution). (b) Residual absorbance spectra of the different films after subtracting plain PCPDTBT and PC₇₁BM spectra in the corresponding ratio from the blend film spectra. The residual spectra fitted (green solid lines) with Gaussian shaped single-band absorption spectra (red curves) representing different vibrational states in ordered polymer structures. (c) Exciton bandwidths W corresponding to the different films without (full symbols) and with (open symbols) ODT. Error bars are deduced from an estimated deviation of 10% for n_{0-0}/n_{0-1} .

The films with ODT (dotted lines) show a pronounced absorption maximum at 800 nm. This feature is missing in the UV/vis data of films without ODT (solid lines) and causes a strongly blue-shifted absorption if no ODT is applied. It arises most probably from missing absorption bands as a result of a lower overall degree of crystallinity as compared to the films with ODT. The absorption spectra of a pure PC₇₁BM film and of a (amorphous) PCPDTBT solution in CB have been measured. They have been weighted according to the sample blend ratios and then been subtracted from the blend film spectra. Hereby, the overall scale of the subtracted spectra of

the amorphous materials was chosen to minimize the baseline of the residual spectra. In a first approximation, the residual spectra then resemble the absorbance that arises from well-ordered polymer structures. The residual spectra are shown in Figure 3b and clearly show that the most probable A_{0-1} photo excitation occurs at lower energies (1.55 eV instead of 1.6 eV) when ODT is used. This observation is a strong qualitative indication for a higher degree of polymer order in the presence of the solvent additive and can be explained by an elongated conjugation length. To support this statement quantitatively, we fitted the residual spectra in the region of polymer absorption using Gaussian-shaped absorption bands (using fityk).³⁹ In this approach, a mutual width and energy offset between the Gaussians is used. The data are shown, along with the fits, in Figure 3b. Typically, the strongest contribution at 1.6 and 1.55 eV (without and with use of ODT, respectively) is identified as the A_{0-1} transition because the first vibronic state is most strongly excited via the A_{0-1} transition. Thus, the band with lower energy corresponds to the A_{0-0} transition. For energies lower than 1.3 eV, no fitting is performed as the nonvanishing baseline most probably arises from reflections at the air/thin film interface. This analysis allows for a comparison of the free exciton bandwidths W via eq 2⁴⁰

$$\frac{A_{0-0}}{A_{0-1}} \approx \frac{n_{0-0}}{n_{0-1}} \left(\frac{1 - 0.24 \frac{W}{E_p}}{1 + 0.073 \frac{W}{E_p}} \right)^2 \quad (2)$$

where n_i are the (real) refractive indices at the respective absorption bands and E_p is the phonon energy of electronically excited state. E_p is determined by the chemical structure of the polymer and thus, is constant for all films. Assuming further that $n_{0-0}/n_{0-1} \approx 1$, eq 2 can be rewritten to eq 3

$$W \propto \frac{W}{E_p} \approx \frac{1 - \sqrt{\frac{A_{0-0}}{A_{0-1}}}}{0.073 \sqrt{\frac{A_{0-0}}{A_{0-1}}} + 0.24} \quad (3)$$

which allows for a comparison of exciton band widths for the different films under investigation. The calculated values are plotted in Figure 3c, whereby a maximum deviation of 10% is assumed for n_{0-0}/n_{0-1} . When no ODT is used, we find a clear trend toward higher exciton bandwidths with increasing polymer content. Since the exciton bandwidth grows with decreasing degree of order in the polymer these findings suggest that a higher polymer fraction without ODT actually reduces the degree of order in the polymer domains. This finding reflects the GIWAXS results where shrinking π - π stacks are found with increasing polymer contents. The exciton bandwidths in films prepared with ODT are less dependent on the film composition and always lower than the ones of the films without ODT. This finding is noteworthy for two reasons: First, it confirms the GIWAXS results and indicates an enhanced crystallinity in case ODT is used and second, it gives first evidence that the morphology might become less sensitive to the polymer weight fraction when ODT is used.

3.2. Mesoscale Morphology. Vertical Composition and Enrichment Layers. The findings on the crystallite length scale suggest that ODT enhances microphase separation, which can lead to the formation of both, vertical and lateral structures. To investigate the vertical film composition and to detect potential enrichment layers, we have performed X-ray reflectivity (XRR) measurements of the blend layers and evaluated them using the

Motofit package by A. Nelson.⁴¹ Reflectivity measurements have been taken at the Copper K_{α} -line (8.048 keV) and thus all scattering length densities (SLDs) are given for this energy. A best fit to the XRR data is obtained by modeling the blend layer, which is applied by a single spin-coating step, as a stack of three distinct sub layers on top of the substrate. Such a model stack is depicted in Figure 4a.

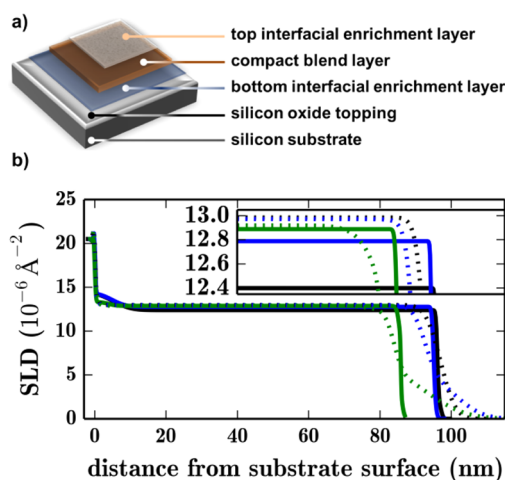


Figure 4. (a) XRR fitting model of the blend layer consisting of three distinct sub layers on top of the substrate. (b) SLD profiles showing film composition of the blend layers as obtained from XRR fitting with respect to the given model. Solid and dotted lines correspond to the films without and with 3 vol % ODT, respectively. Line colors represent the different weight fractions: 1:1.5 (black), 1:2.0 (blue), and 1:2.7 (green). The inset displays a zoom-in for better legibility in the compact layer region.

The first of these sub layers is an interfacial enrichment layer that forms on top of the oxide-topped silicon substrate. It turns over to a compact blend layer with uniform SLD after a certain distance to the substrate surface. This compact blend layer is the second sub layer and displays the main component of the thin film. The third (enrichment) layer on top of the film forms the interface to air. An overview of the film composition along the surface normal as obtained from fitting is given in Figure 4b (for XRR data and fitting curves see Figure S1). We find a first difference between the films with and without ODT in the enrichment layer at the substrate. In case ODT is used, this enrichment layer is slightly above 1 nm thick, regardless of the blend ratio, whereas it spans over roughly 5 nm in the films without ODT. The SLD values of these enrichment layers do not show a clear trend and evaluate to $(14.0 \pm 0.4) \times 10^{-6} \text{ \AA}^{-2}$. Although this value exceeds the ones of thin films from PCPDTBT ($\text{SLD}_{\text{PCPDTBT}} = 10.2 \times 10^{-6} \text{ \AA}^{-2}$) and PC₇₁BM ($\text{SLD}_{\text{PC71BM}} = 13.9 \times 10^{-6} \text{ \AA}^{-2}$), as obtained from XRR measurements of pure materials, no reliable statement on the material composition close to the surface can be given. However, since an enrichment layer similar to the one in films with use of ODT is found in the pure PCPDTBT sample, this layer might consist mostly of the polymer. The higher SLD could be explained by a dense packing and crystallization due to interfacial interactions with the substrate. A closer investigation of the compact layer shows a clear trend for the case where no ODT is used. The SLD increases with the PC₇₁BM weight fraction, reading $12.4(1) \times 10^{-6} \text{ \AA}^{-2}$ (1:1.5), $12.8(1) \times 10^{-6} \text{ \AA}^{-2}$ (1:2.0), and $12.9(2) \times 10^{-6} \text{ \AA}^{-2}$ (1:2.7). For comparison,

the weighted average SLD values for blend layers are calculated from the given weight fractions from the SLDs of pure polymer and fullerene. These theoretical values are $12.4 \times 10^{-6} \text{ \AA}^{-2}$ (1:1.5), $12.7 \times 10^{-6} \text{ \AA}^{-2}$ (1:2.0), and $12.9 \times 10^{-6} \text{ \AA}^{-2}$ (1:2.7) and agree very well with the ones obtained from XRR fitting. Therefore, we conclude that, in the case where no ODT is used, the main part of the blend layer is a vertically homogeneously well intermixed blend film with a polymer:fullerene mixing ratio determined by the amounts used in the solution. The layers further show a sharp surface interface with a width of 1 nm or less. In contrast, films with ODT display a smeared out film surface, where the interface between air and the compact layer spreads out over more than 10 nm. This is in good agreement with AFM measurements published by Peet et al.²² Unlike the films without ODT, the compact layers of the films with ODT show no variation in its SLD ($13.0(1) \times 10^{-6} \text{ \AA}^{-2}$) for all three probed polymer:fullerene ratios. This value is in any case larger than the theoretical values for the different compositions, which most probably arises from an increased degree of polymer crystallinity as compared to ODT-free films. Residual ODT (calculated SLD = $9.1 \times 10^{-6} \text{ \AA}^{-2}$) and polymer crystallization could, however, lead to slight deviations from the calculated values. Because information on the residual ODT content is not accessible, the compact layer composition cannot be reliably determined from the SLD when ODT is used. Nevertheless, for the case that ODT and crystallinity affected all compact layers in the same way, we present the following tentative model: ODT reduces the solubility of PC₇₁BM in the PCPDTBT matrix such, that in all blend ratios, the solubility limit of PC₇₁BM is exceeded. This assumption is based on the fact that all results presented by this work suggest that the morphology becomes less dependent on the blending ratio when ODT is used. In this model, excessive fullerene molecules would agglomerate. Such a behavior has been formerly reported as a consequence of thermal annealing in other polymer:fullerene blend films.^{42–44} In this case, a compact layer with the saturation concentration of PC₇₁BM would form, explaining the common SLD in all compact layers where ODT is used. Excessive fullerene would need to be expelled from the compact layer, either toward the interface between substrate and compact layer or toward the surface. Since the SLD of the accumulation layer at the substrate interface is very similar in both cases, with and without ODT, fullerene molecules would rather be forced toward the film surface, explaining also the rough surface as observed by AFM (by Peet et al.) and XRR.²² The roughness hereby leads to the lower SLD value as compared to pure fullerene. In this case, the fullerene topping would act as a built-in electron transport layer and suppress nongeminate recombination at the contact interfaces, leading to the typical improvement of all photovoltaic parameters as found for PCPDTBT-based solar cells processed with ODT. Indeed, an enhanced surface coverage with fullerene molecules (2% as cast vs 60% with ODT) as well as a strongly suppressed leakage current due to the use of ODT has formerly been suggested by Guerrero et al. based on variable-angle spectroscopic ellipsometry and capacity-voltage measurements.⁴⁵

Lateral Structure. Finally, the lateral structure of the BHJ, which has a strong impact on device performance, is investigated. A well intermixed layer will provide efficient exciton splitting but strong nongeminate recombination, causing low fill factors. In opposite, strong phase separation will lead to large domains which inhibit charge carrier

separation and therefore deteriorate the short-circuit current. In order to probe the mesoscale lateral structure of blend films we performed GISAXS measurements.^{29,46} Representative two-dimensional (2D) scattering images of the films with a blend ratio of 1:2.7 without and with ODT are shown in Figure 5a and b, respectively.

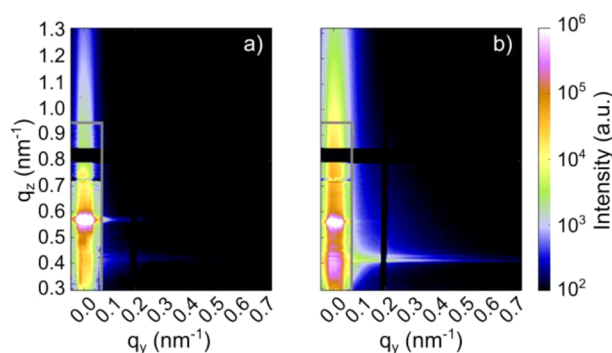


Figure 5. Example of 2D GISAXS data of PCPDTBT:PC₇₁BM (1:2.7) films prepared from CB (a) without and (b) with the addition of 3 vol % ODT. In the Yoneda region ($q_z \approx 0.4 \text{ nm}^{-1}$), strongly enhanced scattering intensity can be found in the case where ODT was added. All data have been corrected for the semitransparent beamstop indicated by the gray rectangle.

Because a semitransparent beamstop was used to protect the detector from overexposure in the specular plane at small angles and to allow simultaneously for reasonable counting rates of laterally scattered X-ray photons, all GISAXS data have been linearly corrected for the absorption of the beamstop (see Figure S2). A clear Yoneda peak from the polymer appears for all samples at the critical angle of 0.17° (PCPDTBT) with respect to the sample surface.⁴⁷ At this critical angle, the scattering signal that arises from the polymer structure is strongly enhanced, which allows for material sensitive analysis of the active layer morphology. By extracting horizontal line cuts from the 2D GISAXS data around the critical angle, we focus on the scattering signal caused by lateral structures of polymer domains within the active blend layer. These horizontal line cuts are depicted in Figure 6.

The solid symbols refer to the films in case no solvent additive was used whereas open symbols are associated with the films that have been processed with the use of ODT. The latter ones show, in contrast to the films without use of ODT, pronounced shoulders in the intensity around $q_y \approx 0.02 \text{ nm}^{-1}$ and $q_y > 0.1 \text{ nm}^{-1}$ in the horizontal line cuts (marked with arrows in Figure 6). Moreover, a general increase of scattering intensity is seen for the samples with added ODT. Therefore, we propose that ODT enhances the microphase separation of PCPDTBT and PC₇₁BM, causing both an increase in the scattering contrast by purifying the domains (due to the different scattering length densities) and an enlargement of pure material domains. A similar mechanism was proposed for blend films based on the other acceptor material PC₆₁BM by Gu et al.²⁴ To estimate the absolute length scales of the domains present inside the films, the horizontal line cuts are modeled within the framework of the distorted wave born approximation (DWBA). A best fit is obtained by modeling the horizontal line cuts by three independent sub structures within the local monodisperse approximation (LMA).⁴⁸ The corre-

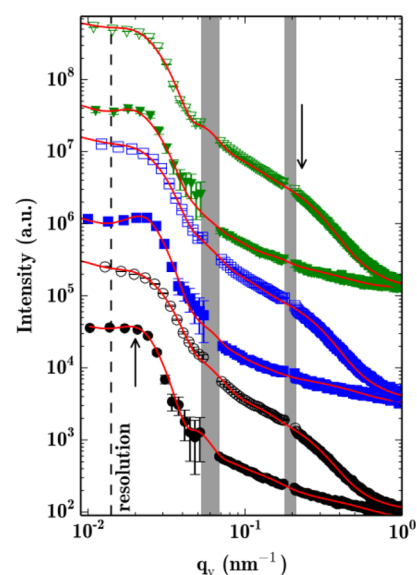


Figure 6. Horizontal line cuts from the 2D GISAXS data (symbols) and model curves (red lines) from films with different compositions: From bottom to top (group wise shifted for clarity): 1:1.5 (black circles), 1:2.0 (blue squares) and 1.2:7 (green triangles). Full symbols represent films where no ODT is used. Open symbols correspond to films where ODT is added. The dashed line marks the resolution limit of the scattering setup toward large scale structures. Data points with $q_y < 0.07 \text{ nm}^{-1}$ have been corrected for the absorption of the semitransparent beamstop. The missing data points (denoted by gray boxes) around 0.06 and 0.2 nm^{-1} arise from the beamstop edges and the inter detector array gap (Dektris PILATUS3 1M), respectively.

sponding model curves are plotted as red lines, together with the horizontal line cuts in Figure 6.

From this analysis, we find that the first shoulder at low $q_y \approx 0.02 \text{ nm}^{-1}$ values originates from the first sub structure describing rather large domains with radii around $75\text{--}90 \text{ nm}$. These object sizes are always slightly smaller when ODT is used. Based on a recent study by Liao et al., where amorphous polymer domains with a fractal radius of around 137 nm were found for blend films with a similar solvent additive (DIO), we identify these objects as amorphous polymer domains.⁴⁹ However, these domains are expected to have only minor influence on photovoltaic characteristics as they are amorphous and show much larger dimensions than typical values of exciton diffusion lengths on the order of up to a few 10 nm in OPV polymers.^{10,50} The second, broad, shoulder at larger $q_y > 0.1 \text{ nm}^{-1}$ values is modeled by the other two substructures which describe domains with mean radii between 5 and around 20 nm in the case where ODT is used. If no ODT is used, the corresponding domain sizes are found to be only half, i.e., in the range of 2.5 to 10 nm . Hereby, domain sizes seem to slightly grow with increasing fullerene content when no ODT is used. In contrast, no trend is observed with ODT (a full overview of the morphological parameters from GISAXS is given in Figure S3). Such findings are a clear sign for enhanced microphase separation caused by ODT addition. As the domain sizes are comparable to typical reported exciton diffusion lengths, we propose that the strong increase of OPV performance is attributed to the increase of domain sizes in the range of a few nanometers. Within this model, the two materials are too well intermixed in films where no ODT is used such that domains show insufficient percolation. Further, too strong intermixing of the materials is expected to hinder polymer crystallite formation

and thus decrease the conductivity within polymer domains, which also leads to lower OPV performance.

4. DISCUSSION—THE FULL IMAGE

All together, the morphological investigations presented in this work can be summed up as shown in Figure 7.

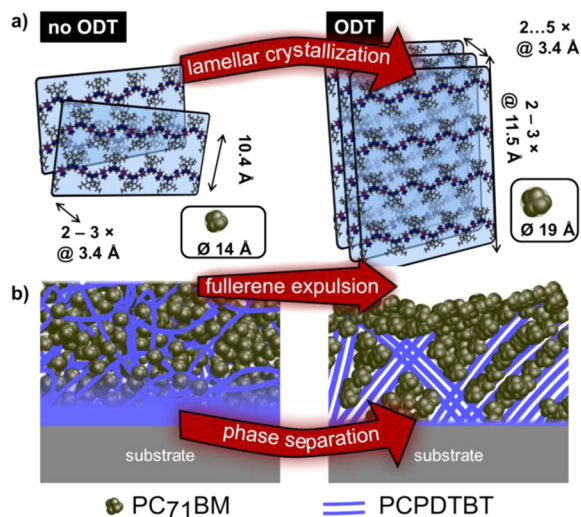


Figure 7. Schematic representation of the PCPDTBT:PC₇₁BM thin film morphology with and without ODT. (a) ODT enhances lamellar crystallization and increases the lamellar packing distance but disturbs π - π stacking. The PC₇₁BM agglomerates are slightly larger with ODT. (b) ODT compactifies the blend layer and expels PC₇₁BM to the surface. Furthermore, it enhances lateral phase segregation on a mesoscopic scale.

Figure 7a hereby denotes the findings about the crystalline structure. We find that the presence of ODT elongates the lamellar stacking distance and leads to formation of lamellar stacks expanding over 2–3 lamellae in case ODT is used. The stack size hereby increases with increasing polymer content. Franck–Condon analysis on UV/vis measurements supports the finding and reveals improved crystallinity when ODT is used. We attribute the increase of both fill factor and short-circuit current of OPV devices published on photovoltaic devices to these results.^{22,51} A further contribution to enhanced power conversion characteristics by use of ODT arises from the vertical film composition, which is indicated in Figure 7b. The film surface has a higher roughness as compared to films without ODT. The scattering length density of the compact film is in this case independent of the blend composition. We suggest that in films with ODT the solubility of fullerene in the polymer matrix is lowered, thus fullerene molecules are expelled toward the surface. This scenario confirms the higher surface coverage of blend films with fullerene molecules as reported by Guerrero et al. and explains a reduction of leakage currents.⁴⁵ An interesting observation made in all scattering experiments is that both the lateral and vertical nanometer-scaled morphology in all probed films becomes less independent of the blend composition when ODT is incorporated. This observation suggests that the increase of short-circuit current with increasing fullerene content as shown by Hwang et al. might be mostly driven by a dense fullerene capping layer that forms when fullerene is expelled from the compact layer and acts as a built-in electron transport layer when ODT is used. Hereby, the fill factor remained constant

and exceeded the one in the case where no ODT is used.⁵¹ We attribute the low fill factor of devices without ODT to the lateral nanometer-scaled morphology. In the case where no ODT is used, the films show excessive mixing, which could lead to formation of fullerene islands that then do not percolate anymore and therefore give rise to strong nongeminate recombination. ODT shows to strongly enhance microphase separation. Thus, the probability for domains to percolate increases and recombination is suppressed as reported by Li et al.⁵²

5. CONCLUSION

In conclusion, we have analyzed the morphology of PCPDTBT:PC₇₁BM blend thin films for use in organic photovoltaics. The influence of the blend ratio (1:1.5, 1:2.0, and 1:2.7) as well as of the addition of 3 vol % ODT is probed by means of X-ray scattering and optical spectroscopy. ODT turns out to enhance microphase separation for all probed blend composition and leads to roughly double domain sizes on a length scale of ten nanometers. ODT boosts lamellar crystallization of PCPDTBT and leads to an increase of overall crystallinity and optical absorbance. It also induces vertical phase separation and leads to formation of a fullerene-rich topping layer on the compact blend layer which acts as built-in electron blocking layer. All together, the use of ODT gives rise to a morphology in which leaking currents and charge recombination are suppressed and thus enhances OPV performance. Keeping this in mind, it is clear that solvent additives provide a simple pathway for optimization of organic solar cells by tuning the nanometer-scaled active layer morphology. Nevertheless, it should be taken into account that the use of solvent additives might have a strong influence on the morphological degradation behavior of the active layer. Finally, the active layer morphology has, once more, proven to be of prime importance when it comes to OPV efficiencies.

■ ASSOCIATED CONTENT

Supporting Information

The Supporting Information is available free of charge on the ACS Publications website at DOI: 10.1021/acsami.5b05939.

XRR data and fitting curves (Figure S1), vertical line cuts of 2D GISAXS data (Figure S2), and full set of fitting parameters determined from the analysis of the GISAXS data (Figure S3) (PDF)

■ AUTHOR INFORMATION

Corresponding Author

*E-mail: muellerb@ph.tum.de. Fax: +49 (0)89 289 12473. Tel: +49 (0)89 289 12451.

Author Contributions

All authors have given approval to the final version of the manuscript.

Funding

TUM.solar in the frame of the Bavarian Collaborative Research Project “Solar technologies go Hybrid” (SolTec), the Green-Tech Initiative (Interface Science for Photovoltaics, ISPV) of the EuroTech Universities, the Nanosystems Initiative Munich (NIM), the China Scholarship Council (CSC), the Erasmus Mundus “MaMaSELF” program, the Bavarian State Ministry of Education, Science and the Arts via the International Graduate School “Materials Science of Complex Interfaces” (CompInt)

Notes

The authors declare no competing financial interest.

ACKNOWLEDGMENTS

This work is financially supported by TUM.solar in the frame of the Bavarian Collaborative Research Project “Solar technologies go Hybrid” (SolTec), the GreenTech Initiative (Interface Science for Photovoltaics, ISPV) of the EuroTech Universities and the Nanosystems Initiative Munich (NIM). B.S. acknowledges funding by the China Scholarship Council (CSC), E.D.I. by the Erasmus Mundus “MaMaSELF” program. C.J.S. acknowledges the Bavarian State Ministry of Education, Science and the Arts via the International Graduate School “Materials Science of Complex Interfaces” (CompInt). We thank D. Magerl for introducing the fitting model for horizontal line cuts in 2D GISAXS data.

REFERENCES

- (1) Dennler, G.; Scharber, M. C.; Brabec, C. J. Polymer-Fullerene Bulk-Heterojunction Solar Cells. *Adv. Mater.* **2009**, *21* (13), 1323–1338.
- (2) Kaltenbrunner, M.; White, M. S.; Glowacki, E. D.; Sekitani, T.; Someya, T.; Sariciftci, N. S.; Bauer, S. Ultrathin and Lightweight Organic Solar Cells with High Flexibility. *Nat. Commun.* **2012**, *3*, 770.
- (3) Dong, Q.; Zhou, Y.; Pei, J.; Liu, Z.; Li, Y.; Yao, S.; Zhang, J.; Tian, W. All-Spin-Coating Vacuum-Free Processed Semi-Transparent Inverted Polymer Solar Cells with PEDOT:PSS Anode and PAH-D Interfacial Layer. *Org. Electron.* **2010**, *11* (7), 1327–1331.
- (4) Chen, C.-C.; Dou, L.; Gao, J.; Chang, W.-H.; Li, G.; Yang, Y. High-Performance Semi-Transparent Polymer Solar Cells Possessing Tandem Structures. *Energy Environ. Sci.* **2013**, *6*, 2714–2720.
- (5) Søndergaard, R.; Hösel, M.; Angmo, D.; Larsen-Olsen, T. T.; Krebs, F. C. Roll-to-Roll Fabrication of Polymer Solar Cells. *Mater. Today* **2012**, *15* (1–2), 36–49.
- (6) Schubert, D. W.; Dunkel, T. Spin Coating from a Molecular Point of View: Its Concentration Regimes, Influence of Molar Mass and Distribution. *Mater. Res. Innovations* **2003**, *7* (5), 314–321.
- (7) Vak, D.; Kim, S.-S.; Jo, J.; Oh, S.-H.; Na, S.-I.; Kim, J.; Kim, D.-Y. Fabrication of Organic Bulk Heterojunction Solar Cells by a Spray Deposition Method for Low-Cost Power Generation. *Appl. Phys. Lett.* **2007**, *91* (8), 081102.
- (8) Ruderer, M. A.; Meier, R.; Porcar, L.; Cubitt, R.; Müller-Buschbaum, P. Phase Separation and Molecular Intermixing in Polymer–Fullerene Bulk Heterojunction Thin Films. *J. Phys. Chem. Lett.* **2012**, *3* (6), 683–688.
- (9) Markov, D. E.; Amsterdam, E.; Blom, P. W. M.; Sieval, A. B.; Hummelen, J. C. Accurate Measurement of the Exciton Diffusion Length in a Conjugated Polymer Using a Heterostructure with a Side-Chain Cross-Linked Fullerene Layer. *J. Phys. Chem. A* **2005**, *109* (24), 5266–5274.
- (10) Shaw, P. E.; Ruseckas, A.; Samuel, I. D. W. Exciton Diffusion Measurements in Poly(3-Hexylthiophene). *Adv. Mater.* **2008**, *20* (18), 3516–3520.
- (11) Hoppe, H.; Sariciftci, N. S. Organic Solar Cells: An Overview. *J. Mater. Res.* **2004**, *19* (07), 1924–1945.
- (12) Brabec, C. J.; Sariciftci, N. S.; Hummelen, J. C. Plastic Solar Cells. *Adv. Funct. Mater.* **2001**, *11* (1), 15–26.
- (13) Brabec, C. J.; Gowrisanker, S.; Halls, J. J. M.; Laird, D.; Jia, S.; Williams, S. P. Polymer–Fullerene Bulk-Heterojunction Solar Cells. *Adv. Mater.* **2010**, *22* (34), 3839–3856.
- (14) Li, G.; Zhu, R.; Yang, Y. Polymer Solar Cells. *Nat. Photonics* **2012**, *6* (3), 153–161.
- (15) Kim, Y.; Choulis, S. A.; Nelson, J.; Bradley, D. D. C.; Cook, S.; Durrant, J. R. Device Annealing Effect in Organic Solar Cells with Blends of Regioregular poly(3-Hexylthiophene) and Soluble Fullerene. *Appl. Phys. Lett.* **2005**, *86* (6), 063502.
- (16) Li, G.; Shrotriya, V.; Huang, J.; Yao, Y.; Moriarty, T.; Emery, K.; Yang, Y. High-Efficiency Solution Processable Polymer Photovoltaic Cells by Self-Organization of Polymer Blends. *Nat. Mater.* **2005**, *4* (11), 864–868.
- (17) Clarke, T. M.; Ballantyne, A. M.; Nelson, J.; Bradley, D. D. C.; Durrant, J. R. Free Energy Control of Charge Photogeneration in Polythiophene/Fullerene Solar Cells: The Influence of Thermal Annealing on P3HT/PCBM Blends. *Adv. Funct. Mater.* **2008**, *18* (24), 4029–4035.
- (18) Wang, T.; Pearson, A. J.; Dunbar, A. D. F.; Staniec, P. A.; Watters, D. C.; Yi, H.; Ryan, A. J.; Jones, R. A. L.; Iraqi, A.; Lidzey, D. G. Correlating Structure with Function in Thermally Annealed PCDTBT:PC70BM Photovoltaic Blends. *Adv. Funct. Mater.* **2012**, *22* (7), 1399–1408.
- (19) Li, G.; Yao, Y.; Yang, H.; Shrotriya, V.; Yang, G.; Yang, Y. “Solvent Annealing” Effect in Polymer Solar Cells Based on Poly(3-Hexylthiophene) and Methanofullerenes. *Adv. Funct. Mater.* **2007**, *17* (10), 1636–1644.
- (20) Ruderer, M. A.; Guo, S.; Meier, R.; Chiang, H.-Y.; Körstgens, V.; Wiedersich, J.; Perlich, J.; Roth, S. V.; Müller-Buschbaum, P. Solvent-Induced Morphology in Polymer-Based Systems for Organic Photovoltaics. *Adv. Funct. Mater.* **2011**, *21* (17), 3382–3391.
- (21) Liang, Y.; Xu, Z.; Xia, J.; Tsai, S.-T.; Wu, Y.; Li, G.; Ray, C.; Yu, L. For the Bright Future—Bulk Heterojunction Polymer Solar Cells with Power Conversion Efficiency of 7.4%. *Adv. Mater.* **2010**, *22* (20), E135–E138.
- (22) Peet, J.; Kim, J. Y.; Coates, N. E.; Ma, W. L.; Moses, D.; Heeger, A. J.; Bazan, G. C. Efficiency Enhancement in Low-Bandgap Polymer Solar Cells by Processing with Alkane Dithiols. *Nat. Mater.* **2007**, *6* (7), 497–500.
- (23) Peet, J.; Soci, C.; Coffin, R. C.; Nguyen, T. Q.; Mikhailovsky, A.; Moses, D.; Bazan, G. C. Method for Increasing the Photoconductive Response in Conjugated Polymer/fullerene Composites. *Appl. Phys. Lett.* **2006**, *89* (25), 252105.
- (24) Gu, Y.; Wang, C.; Russell, T. P. Multi-Length-Scale Morphologies in PCPDTBT/PCBM Bulk-Heterojunction Solar Cells. *Adv. Energy Mater.* **2012**, *2* (6), 683–690.
- (25) Wienk, M. M.; Kroon, J. M.; Verhees, W. J. H.; Knol, J.; Hummelen, J. C.; van Hal, P. A.; Janssen, R. A. J. Efficient Methano[70]fullerene/MDMO-PPV Bulk Heterojunction Photovoltaic Cells. *Angew. Chem.* **2003**, *115* (29), 3493–3497.
- (26) Park, S. H.; Roy, A.; Beaupre, S.; Cho, S.; Coates, N.; Moon, J. S.; Moses, D.; Leclerc, M.; Lee, K.; Heeger, A. J. Bulk Heterojunction Solar Cells with Internal Quantum Efficiency Approaching 100%. *Nat. Photonics* **2009**, *3* (5), 297–302.
- (27) Wang, D. H.; Kim, D. Y.; Choi, K. W.; Seo, J. H.; Im, S. H.; Park, J. H.; Park, O. O.; Heeger, A. J. Enhancement of Donor–Acceptor Polymer Bulk Heterojunction Solar Cell Power Conversion Efficiencies by Addition of Au Nanoparticles. *Angew. Chem.* **2011**, *123* (24), 5633–5637.
- (28) Müller-Buschbaum, P. The Active Layer Morphology of Organic Solar Cells Probed with Grazing Incidence Scattering Techniques. *Adv. Mater.* **2014**, *26* (46), 7692–7709.
- (29) Hexemer, A.; Müller-Buschbaum, P. Advanced Grazing-Incidence Techniques for Modern Soft-Matter Materials Analysis. *IUCr* **2015**, *2* (1), 106–125.
- (30) Baker, J. L.; Jimison, L. H.; Mansfeld, S.; Volkman, S.; Yin, S.; Subramanian, V.; Salleo, A.; Alivisatos, A. P.; Toney, M. F. Quantification of Thin Film Crystallographic Orientation Using X-Ray Diffraction with an Area Detector. *Langmuir* **2010**, *26* (11), 9146–9151.
- (31) Verploegen, E.; Miller, C. E.; Schmidt, K.; Bao, Z.; Toney, M. F. Manipulating the Morphology of P3HT–PCBM Bulk Heterojunction Blends with Solvent Vapor Annealing. *Chem. Mater.* **2012**, *24* (20), 3923–3931.
- (32) Rogers, J. T.; Schmidt, K.; Toney, M. F.; Kramer, E. J.; Bazan, G. C. Structural Order in Bulk Heterojunction Films Prepared with Solvent Additives. *Adv. Mater.* **2011**, *23* (20), 2284–2288.

- (33) Müller-Buschbaum, P. Influence of Surface Cleaning on Dewetting of Thin Polystyrene Films. *Eur. Phys. J. E: Soft Matter Biol. Phys.* **2003**, *12* (3), 443–448.
- (34) Jiang, Z. GIXSGUI: A MATLAB Toolbox for Grazing-Incidence X-Ray Scattering Data Visualization and Reduction, and Indexing of Buried Three-Dimensional Periodic Nanostructured Films. *J. Appl. Crystallogr.* **2015**, *48* (3), 917–926.
- (35) Van Der Gaast, S. J. A Method to Eliminate the Background in X-Ray Diffraction Patterns of Oriented Clay Mineral Samples. *Clay Miner.* **1981**, *16* (4), 383–393.
- (36) Hedberg, K.; Hedberg, L.; Bühl, M.; Bethune, D. S.; Brown, C. A.; Johnson, R. D. Molecular Structure of Free Molecules of the Fullerene C70 from Gas-Phase Electron Diffraction. *J. Am. Chem. Soc.* **1997**, *119* (23), 5314–5320.
- (37) Erb, T.; Zhokhavets, U.; Gobsch, G.; Raleva, S.; Stühn, B.; Schilinsky, P.; Waldauf, C.; Brabec, C. J. Correlation Between Structural and Optical Properties of Composite Polymer/Fullerene Films for Organic Solar Cells. *Adv. Funct. Mater.* **2005**, *15* (7), 1193–1196.
- (38) Palumbiny, C. M.; Liu, F.; Russell, T. P.; Hexemer, A.; Wang, C.; Müller-Buschbaum, P. The Crystallization of PEDOT:PSS Polymeric Electrodes Probed In Situ during Printing. *Adv. Mater.* **2015**, *27* (22), 3391–3397.
- (39) Wojdyr, M. Fityk: A General-Purpose Peak Fitting Program. *J. Appl. Crystallogr.* **2010**, *43* (5), 1126–1128.
- (40) Spano, F. C. Modeling Disorder in Polymer Aggregates: The Optical Spectroscopy of Regioregular poly(3-Hexylthiophene) Thin Films. *J. Chem. Phys.* **2005**, *122* (23), 234701.
- (41) Nelson, A. Co-Refinement of Multiple-Contrast neutron/X-Ray Reflectivity Data Using MOTOFIT. *J. Appl. Crystallogr.* **2006**, *39* (2), 273–276.
- (42) Richards, J. J.; Rice, A. H.; Nelson, R. D.; Kim, F. S.; Jenekhe, S. A.; Luscombe, C. K.; Pozzo, D. C. Modification of PCBM Crystallization via Incorporation of C60 in Polymer/Fullerene Solar Cells. *Adv. Funct. Mater.* **2013**, *23* (4), 514–522.
- (43) Ma, W.; Yang, C.; Gong, X.; Lee, K.; Heeger, A. J. Thermally Stable, Efficient Polymer Solar Cells with Nanoscale Control of the Interpenetrating Network Morphology. *Adv. Funct. Mater.* **2005**, *15* (10), 1617–1622.
- (44) Hoppe, H.; Sariciftci, N. S. Morphology of Polymer/fullerene Bulk Heterojunction Solar Cells. *J. Mater. Chem.* **2006**, *16* (1), 45–61.
- (45) Guerrero, A.; Dörfling, B.; Ripolles-Sanchis, T.; Aghamohammadi, M.; Barrena, E.; Campoy-Quiles, M.; Garcia-Belmonte, G. Interplay between Fullerene Surface Coverage and Contact Selectivity of Cathode Interfaces in Organic Solar Cells. *ACS Nano* **2013**, *7* (5), 4637–4646.
- (46) Müller-Buschbaum, P. Grazing Incidence Small-Angle X-Ray Scattering: An Advanced Scattering Technique for the Investigation of Nanostructured Polymer Films. *Anal. Bioanal. Chem.* **2003**, *376* (1), 3–10.
- (47) Yoneda, Y. Anomalous Surface Reflection of X Rays. *Phys. Rev.* **1963**, *131* (5), 2010–2013.
- (48) Lazzari, R. IsGISAXS: A Program for Grazing-Incidence Small-Angle X-Ray Scattering Analysis of Supported Islands. *J. Appl. Crystallogr.* **2002**, *35* (4), 406–421.
- (49) Liao, H.-C.; Tsao, C.-S.; Shao, Y.-T.; Chang, S.-Y.; Huang, Y.-C.; Chuang, C.-M.; Lin, T.-H.; Chen, C.-Y.; Su, C.-J.; Jeng, U. S.; Chen, Y.-F.; Su, W.-F. Bi-Hierarchical Nanostructures of Donor-Acceptor Copolymer and Fullerene for High Efficient Bulk Heterojunction Solar Cells. *Energy Environ. Sci.* **2013**, *6* (6), 1938–1948.
- (50) Mikhnenko, O. V.; Azimi, H.; Scharber, M.; Morana, M.; Blom, P. W. M.; Loi, M. A. Exciton Diffusion Length in Narrow Bandgap Polymers. *Energy Environ. Sci.* **2012**, *5* (5), 6960–6965.
- (51) Hwang, I.-W.; Cho, S.; Kim, J. Y.; Lee, K.; Coates, N. E.; Moses, D.; Heeger, A. J. Carrier Generation and Transport in Bulk Heterojunction Films Processed with 1,8-Octanedithiol as a Processing Additive. *J. Appl. Phys.* **2008**, *104* (3), 033706.
- (52) Li, Z.; McNeill, C. R. Transient Photocurrent Measurements of PCDTBT:PC70BM and PCPDTBT:PC70BM Solar Cells: Evidence for Charge Trapping in Efficient Polymer/fullerene Blends. *J. Appl. Phys.* **2011**, *109* (7), 074513.